

Development of lipoyl-substituted porphyrins as novel biocompatible mitochondria-targeting agents

Apiratt Thitimon^a, Vitavat Aksornkitti^b, Amornpun Sereemasun^b, Patchanita Thamyongkit^a, Vinich Promarak^c, Rojrit Rojanathanes^{a,*}

^a Department of Chemistry, Faculty of Science, Chulalongkorn University, Bangkok 10330 Thailand

^b Nanomedicine Research Unit, Department of Anatomy, Faculty of Medicine, Chulalongkorn University, Bangkok 10330 Thailand

^c School of Molecular Science and Engineering, Vidyasirimedhi Institute of Science and Technology (VISTEC), Rayong 21210 Thailand

*Corresponding author, e-mail: rojrit@hotmail.com

Received 13 Mar 2022, Accepted 1 Jun 2022

Available online 10 Aug 2022

ABSTRACT: This work described synthesis and investigation of a novel water-soluble lipoyl-substituted porphyrin derivative and its Mn(III)-complex for mitochondria-targeting activities. The freebase derivative was obtained in moderate yield from alkylation of 5,10,15,20-tetra(4-pyridyl)porphyrin followed by amidation with lipoic acid anhydride. Mn-metallation of the freebase derivative quantitatively produced the target Mn(III)-porphyrin. Both lipoyl-substituted porphyrin and Mn(III)-complex were fully characterized by NMR spectroscopy, mass spectrometry, absorption spectrophotometry, and emission spectrophotometry. Both compounds were considered to have low cytotoxicity with IC₅₀ values of 29–49 and more than 78 μM, respectively, against the HaCaT and HDFa cells. In addition, mitochondria-targeting evaluation suggested that these target porphyrin derivatives exhibited accumulation, specifically in the mitochondria of the HaCaT cells.

KEYWORDS: porphyrin, lipoic acid, mitochondrial targeting compound, Mn metalation

INTRODUCTION

Mitochondria is a main cellular organelle that performs many important cellular functions. Many cellular activities such as energy production (ATP), metabolism, homeostasis, the cycle of cell growth, replication and death are controlled by mitochondrial function to keep body work properly [1–3]. Mitochondrial disorders caused by effects of oxidative stress from mitochondrial activities can lead to many diseases [4–7]. Hence, the mitochondria become an attractive potential target for the treatment of various human diseases.

Nowadays, numerous porphyrin compounds are of great interest as antioxidants for biomedical applications due to their high chemical stability, easy to enhance biological activity through structural modification, low toxicity, and rapid body clearance [8–10]. In addition, many studies demonstrated that cationic porphyrins have ability to localize and accumulate in the mitochondria [11, 12]. While electrostatic interaction between the cationic porphyrins and negative charges of mitochondrial membrane is a driving force, lipophilicity on a porphyrin ring is another factor that affects their transport across the mitochondrial membrane [13, 14]. Some metal complexes of porphyrins, especially manganese, have been reported not only as remarkable mitochondrial targeting agents due to their highly positive charge in the porphyrin rings [15–18], but also as effective antioxidants in the mitochondria [19–22].

Apart from this, α-Lipoic acid (ALA), one of well-

known biomedically active compounds, plays a vital role in the human mitochondria [23, 24]. ALA can act as an effective antioxidant in preventing mitochondrial dysfunction from oxidative stress [25, 26], works as a cofactor for many enzyme complexes including mitochondrial respiratory enzymes [27], and has been shown to maintain the mitochondrial function as well [28].

The present study focused on the synthesis and characterization of a new porphyrin derivative and its Mn(III)-complex bearing *N*-lipoyl pyridinium meso substituents as mitochondrial targeting agents. Positively charged pyridinium moieties increased water solubility of the porphyrin which, consequently, enabled applications in aqueous media of cell environments. The target molecules are expected to exhibit low cytotoxicity and high specificity to the mitochondria which will be beneficial for the development of future generation of therapeutic agents.

MATERIALS AND METHODS

All reagents and solvents used in the experiments were analytical grade, purchased from Sigma-Aldrich (USA), Fluka (Switzerland), or Merck (Germany) and used as received without further purification. All ¹H-NMR spectra were determined using a Varian Mercury NMR spectrometer operating at 400 MHz for ¹H nuclei, and ¹³C-NMR spectra were determined using a Bruker NMR spectrometer operating at 100 MHz for ¹³C nuclei. Mass spectra were recorded using a Mi-

croflex MALDI-TOF mass spectrometer (Bruker Daltonics) with α -cyano-4-hydroxycinnamic acid (CCA) as a matrix. Absorption spectra and emission spectra were measured at room temperature using a Cary 60 UV-vis spectrophotometer and a Varian Cary Eclipse spectrofluorometer, respectively. The maximum absorption wavelength was used as excitation wavelength of each porphyrin.

Non-commercial compound

The 5,10,15,20-tetra(4-pyridyl)porphyrin (compound 1) [29] (see Supplementary data for full characterization) and *tert*-butyl-*N*-(2-bromoethyl)carbamate [30] were synthesized according to a previous literature procedures. Lipoic acid anhydride solution [31] was prepared following a previous report with slight modification by using acetonitrile instead of dichloromethane.

Synthesis of

5,10,15,20-tetrakis(4-*N*-(2-aminoethyl)pyridyl)porphyrin (compound 2)

A mixture of compound 1 (0.020 g, 0.032 mmol) and *tert*-butyl-*N*-(2-bromoethyl)carbamate (2.0080 g, 8.960 mmol) was stirred at 120 °C for 12 h. After cooling the mixture to room temperature, a brown solid was washed with DMF, ethanol and then acetone in an ultrasonic bath. Subsequently, crude product was precipitated in 6% H₂O in acetone, and purple-brown solid (0.020 g, 56%) was obtained. ¹H-NMR (D₂O) δ : 4.10 (t, *J* = 8.0 Hz, 8H), 5.43 (t, *J* = 8.0 Hz, 8H), 9.14 (d, *J* = 4.0 Hz, 8H), 8.97–9.40 (br, 8H), 9.53 (d, *J* = 4.0 Hz, 8H); ¹³C-NMR (D₂O) δ : 39.6, 58.5, 115.8, 134.1, 143.8, 159.1. The pD value = 7.63. MALDI-TOF-MS obsd 794.782; calcd mass 795.010 ([M]⁺, M = C₄₈H₅₀N₁₂); λ_{abs} (H₂O) 426, 521, 556, 586, 641 nm; λ_{em} (H₂O, λ_{ex} = 426 nm) 711 nm (see Supplementary data for full characterization).

Synthesis of compound 3

A solution of compound 2 (20 mg, 0.018 mmol) in water (2 ml) was added to a solution of lipoic acid anhydride at room temperature under N₂ atmosphere. After 18 h, the resulting mixture was filtered to remove solid byproduct. The solution was poured into acetone to precipitate. The solid was washed several times with acetone to obtain purple-brown solid (25.0 mg, 74%). ¹H-NMR (DMSO-*d*6) δ : -3.09 (s, 2H), 1.21–1.47 (m, 16H), 1.48–1.67 (m, 16H), 1.99–2.11 (m, 4H), 2.22 (t, *J* = 7.2 Hz, 8H), 2.65–2.75 (m, 4H), 2.79–2.90 (m, 4H), 3.94 (br, 8H), 5.02 (br, 8H), 8.49 (t, *J* = 8.0 Hz, 4H), 9.00 (d, *J* = 4.0 Hz, 8H), 9.21 (s, 8H), 9.55 (d, *J* = 4.0 Hz, 8H); ¹³C-NMR (DMSO-*d*6) δ : 24.9, 28.4, 34.0, 35.1, 37.8, 55.8, 61.3, 115.8, 132.1, 143.9, 156.4, 173.5; MALDI-TOF-MS obsd 1548.650; calcd avg mass 1548.222 ([M]⁺, M = C₈₀H₉₈N₁₂O₄S₈); λ_{abs} (H₂O) (ϵ) 430 (1.1 × 10⁵), 525, 560, 593, 649 nm; λ_{em}

(H₂O, λ_{ex} = 430 nm) 658, 721 nm (see Supplementary data for full characterization).

Synthesis of compound Mn-3

Manganese(II) chloride tetrahydrate (38 mg, 0.19 mmol) was added to a solution of compound 3 (10 mg, 0.0053 mmol) in DMF (2 ml) with one drop of triethylamine (TEA) at room temperature under N₂ atmosphere. The reaction was monitored by fluorescence spectroscopy until the emission bands at 658 and 721 nm were completely disappeared (approximately 2 h). Then, the mixture was precipitated by adding diethylether. The solid was washed with diethylether and ethanol to obtain a dark-brown solid (9 mg, 83%). MALDI-TOF-MS obsd 1601.134, 1789.296; calcd mass 1601.144 ([M]⁺, M = C₈₀H₉₈MnN₁₂O₄S₈), 1789.306 ([M+CCA]⁺, M+CCA = C₉₀H₁₀₂MnN₁₃O₇S₈); λ_{abs} (H₂O) 331, 378, 400, (ϵ) 464 (7.7 × 10⁴), 563 nm (see Supplementary data for full characterization).

Cell culture

Following the standard procedure [32], Human dermal fibroblast, adult (HDFa) and Human keratinocyte (HaCaT) cell lines were cultured in DMEM (Gibco, USA) containing 10% (v/v) fetal bovine serum (FBS) (Gibco, USA) and 1% (v/v) antibiotic antimycotic (Gibco, USA) at 37 °C in 5% CO₂. Cells at early passages (below 30 passages) were used in cell experiments to avoid complications of replicative senescence. After the HDFa and HaCaT cell lines reached 90% confluence, cells were sub-cultured using 0.25% trypsin/EDTA (Gibco, USA).

Cytotoxicity test (cell viability)

The cellular cytotoxicity was studied by cell viability assay using PrestoBlue™ reagent (Invitrogen, USA) [33]. HDFa and HaCaT cell lines were seeded into 96-well plates at density of 5 × 10³ cells/well in 100 μ l of complete medium and incubated at 37 °C under 5% CO₂ atmosphere for 12 h. Cells were washed by phosphate buffered saline (PBS) twice and treated with various concentrations of Dulbecco's Modified Eagle Medium (DMEM) which served as the control, ALA (121–727 μ M), compound 3 (13–80 μ M), and Mn-3 (13–78 μ M) for 24 h. Then, 10 μ l of PrestoBlue™ reagent was added into cell and incubated for 30 min. Fluorescence was measured using a microplate reader at 560 and 590 nm (Thermo, Varioskan flash, England). The percentage of cell viability was calculated by normalizing to a control group (DMEM).

Mitochondria targeting evaluation

The mitochondria targeting activity was determined by cell imaging using a LSM 800 confocal microscope. Following a previously published report [34], the HaCaT cells were seeded in 24 wells (Corning) plate at a

1.21–2.90 ppm in the $^1\text{H-NMR}$ spectrum confirmed the formation of compound 3. In addition, the protons on the pyrrole and pyridinium rings of compound 3 exhibited signals at 9.14–9.53 ppm, while characteristic singlet signal of two inner protons in the porphyrin ring appeared at -3.09 ppm. Based on $^{13}\text{C-NMR}$, a signal of carbonyl carbons of the amide groups of compound 3 was found at δ 173.5 ppm, while those of the lipoyl groups appeared at δ 24.9–55.8 ppm. The signals of the aromatic carbons and the alkyl chains on the aminoethyl groups of compound 3 were in a similar region as those of compound 2. Moreover, a MALDI-TOF mass spectrum of compound 3 showed its molecular ion peak $[\text{M}]^+$ at m/z 1548.650.

To obtain the desired water-soluble Mn-3, compound 3 was metallated by manganese(II) chloride tetrahydrate in the presence of triethylamine in DMF at room temperature for 2 h, yielding in 83% dark-brown solid of Mn-3. The formation of Mn-3 was confirmed by UV-visible spectroscopy and MALDI-TOF-MS. Compared with the absorption spectrum of compound 3, the maximum absorption band was shifted from 430 to 464 nm. The two absorption bands at 378 and 400 nm are characteristic bands of Mn(III) species. In addition, disappearance of an emission spectrum of compound 3 indicated complete metallation. Furthermore, a MALDI-TOF mass spectrum showed its molecular ion peaks $[\text{M}]^+$ at m/z 1601.134.

Cytotoxicity

The cytotoxicity of target porphyrin derivatives were evaluated by cell viability assay tested on human keratinocyte immortal (HaCaT) and human dermal fibroblasts adult (HDFa) cell lines. According to properties of the porphyrins and ALA, we expected to develop this molecule for the future generation of applying-on-skin therapeutic agents. Epidermal keratinocytes and HDFa, as part of the outermost layer of the skin and directly exposed to the molecules, may receive side effects. Thus, it is valuable to study dermal toxicity of porphyrins and ALA as a main exposure of nanoparticle to human body. Different concentrations of ALA (121–727 μM), compound 3 (13–80 μM), and Mn-3 (13–78 μM) were administered to cell cultures in Dulbecco's modified Eagle's medium (DMEM), and the cells were incubated in the dark for 24 h. Then, PrestoBlue reagent was added into the cells and incubated for another 30 min, resulting in the formation of fluorescence dye. The percentage of cell viability was calculated with normalized fluorescence signal, compared with a control group as shown in Fig. 1.

Results showed that the cell viability of both HaCaT and HDFa cells treated with ALA was slightly increased with the increased concentration of ALA indicating that ALA exhibited no cytotoxicity in the concentration range studied in this experiment and

might increase enzymatic activity that caused cell proliferation. When the cells were treated with compound 3, decreases in cell viability of both HaCaT and HDFa cells were observed. From the graphs, compound 3 exhibited IC_{50} values of 29 μM and 49 μM against HaCaT and HDFa cells, respectively, while the IC_{50} value against both cell lines was higher than 78 μM upon treatment with Mn-3. This observation suggested that the Mn-chelation of the porphyrin unit could decrease cytotoxicity against the HaCaT and HDFa cells. As in previous reports, Mn-complexes of pyridinyl porphyrins showed low toxicity against various types of cells [20, 21]. Moreover, this decrease in cytotoxicity possibly related to their essential role in development, activation of certain metalloenzymes, energy metabolism, and immunological system function [36].

Mitochondria targeting evaluation

In this study, the mitochondria targeting activities of compound 3 and Mn-3 were determined by cell imaging using a LSM 800 confocal microscope. The HaCaT cells were chosen because of their high capacity to proliferate. In order to indicate positions of cells, nuclei of the HaCaT cells were stained with Hoechst 33342 dye (as seen in the blue fluorescence in Fig. 2). As for mitochondria staining, JC-1 dye was loaded into the HaCaT cells. Generally, JC-1 dye accumulated in mitochondrial matrix exhibits green fluorescence. The transport of various molecules into the mitochondria affects mitochondrial membrane potential and, hence, causes aggregation of JC-1 dyes, which exhibits intensified red fluorescence. Fig. 2A shows that the images of the HaCaT cells treated with only DMEM (control) mainly exhibited green fluorescence with red fluorescence at some parts, indicating that DMEM was slightly accumulated in the mitochondria. Similarly, the cells treated with ALA showed green fluorescence (Fig. 2B), suggesting that ALA did not significantly accumulated in the mitochondria. On the contrary, Fig. 2C shows that the compound-3 treated cells exhibited higher intensity of red fluorescence, compared with the cells treated with ALA. The result suggested that compound 3 could effectively accumulate in the mitochondria, likely due to electrostatic attraction between positively charged porphyrin and negatively charged environment of the mitochondrial inner membrane.

Moreover, upon the treatment with Mn-3, the cells clearly exhibited green and red fluorescence in the same extent as that observed in the cells treated with compound 3 (Fig. 2D), suggesting that Mn-3 could be accumulated in the mitochondria in a similar manner as compound 3. Thus, it can be concluded that the Mn-chelation of compound 3 did not significantly increase the mitochondria-targeting ability, but rather played a role in maintaining the cell viability.

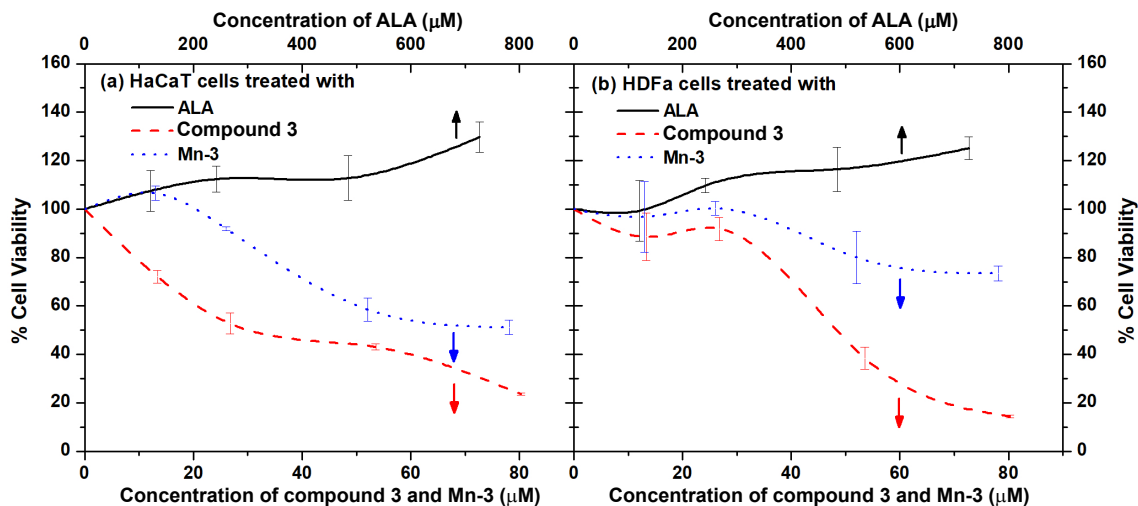


Fig. 1 Cell viability of: (a), HaCaT cells; and (b), HDFa cells treated with various concentrations of ALA (black solid line), compound 3 (red dash line) and Mn-3 (blue dot line) at (ALA on the upper x-axis, compound 3 and Mn-3 on the lower x-axis)

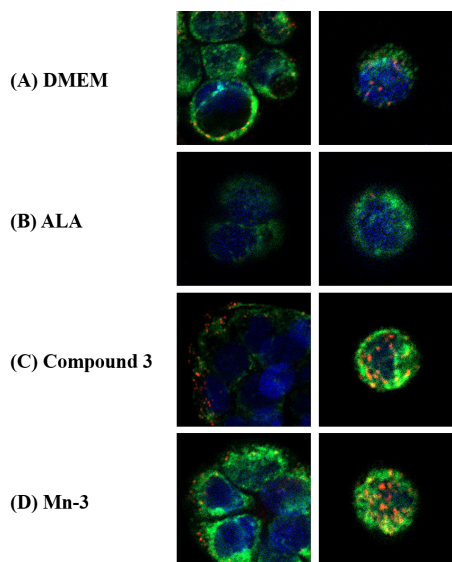


Fig. 2 Images of the HaCaT cell colonies (left) and separate cells (right) treated with: (A), DMEM; (B), ALA; (C), compound 3; (D), Mn-3.

CONCLUSION

The new water-soluble porphyrin derivatives bearing the lipoyl meso-substituents with and without manganese central metal were successfully synthesized. Both compounds exhibited low cytotoxicity in the HaCaT and HDFa cells. In comparison to the freebase derivative, the Mn-chelation on the porphyrin unit tended to decrease the cell cytotoxicity, while did not give significant effect on the mitochondria-targeting activity. Both target porphyrin derivatives exhibited specific accumulation in the mitochondria. The low cy-

tototoxicity and the high specificity to the mitochondria of the target Mn-chelated porphyrins should be beneficial in the development of several new therapeutic approaches in the future.

Appendix A. Supplementary data

Supplementary data associated with this article can be found at <http://dx.doi.org/10.2306/scienceasia1513-1874.2022.113>.

Acknowledgements: This work is supported by The Grant to support a research group in the Ratchadaphiseksomphot Endowment Fund, Chulalongkorn University, Development and Promotion of Science and Technology Talents Project (DPST) and Thai-German S&T Cooperation 3rd Researcher Mobility Scheme 2016 (PORPH-MEB), Grant for Joint Funding, Ratchadaphiseksomphot Endowment Fund, and Thailand Research Fund (RTA6080005).

REFERENCES

1. Fulda S, Galluzzi L, Kroemer G (2010) Targeting mitochondria for cancer therapy. *Nat Rev Drug Discov* **9**, 447–464.
2. Palanisamy AP, Cheng G, Sutter AG, Evans ZP, Polito CC, Jin L, Liu J, Schmidt MG, et al (2014) Mitochondrial uncoupling protein 2 induces cell cycle arrest and necrotic cell death. *Metab Syndr Relat Disord* **12**, 132–142.
3. Rubeai M, Chalder S, Bird R, Emery AN (1991) Cell cycle, cell size and mitochondrial activity of hybridoma cells during batch cultivation. *Cytotechnology* **7**, 179–186.
4. Khambatta S, Nguyen DL, Beckman TJ, Wittich CM (2014) Kearns-Sayre syndrome: a case series of 35 adults and children. *Int J Gen Med* **7**, 325–332.
5. Matthews L, Enzinger C, Fazekas F, Rovira A, Ciccarelli O, Dotti MT, Filippi M, Frederiksen JL, et al (2015) MRI in Leber's hereditary optic neuropathy: the relationship to multiple sclerosis. *J Neurol Neurosurg Psychiatry* **86**, 537–542.

6. Perier C, Vila M (2012) Mitochondrial biology and Parkinson's disease. *Cold Spring Harb Perspect Med* **4**, a009332.
7. Rendon DA (2016) The bioenergetics of isolated mitochondria from different animal models for diabetes. *Curr Diabetes Rev* **12**, 66–80.
8. Hadmojo WT, Yim D, Aqoma H, Ryu DY, Shin TJ, Kim HW, Hwang E, Jang WD, et al (2017) Artificial light-harvesting n-type porphyrin for panchromatic organic photovoltaic devices. *Chem Sci* **8**, 5095–5100.
9. Stojiljkovic I, Evavold BD, Kumar V (2001) Antimicrobial properties of porphyrins. *Exp Opin Invest Drugs* **10**, 309–320.
10. Huang H, Song W, Rieffel J, Lovell JF (2015) Emerging applications of porphyrins in photomedicine. *Front Phys* **3**, ID 23.
11. Engelmann FM, Mayer I, Gabrielli DS, Toma HE, Kowaltowski AJ, Araki K, Baptista MS (2007) Interaction of cationic meso-porphyrins with liposomes, mitochondria and erythrocytes. *J Bioenerg Biomembr* **39**, 175–185.
12. Lei W, Xie J, Hou Y, Jiang G, Zhang H, Wang P, Wang X, Zhang B (2010) Mitochondria-targeting properties and photodynamic activities of porphyrin derivatives bearing cationic pendant. *J Photochem Photobiol B Biol* **98**, 167–171.
13. Cerney T, Zimmermann HW (1996) Selective photosensitization of mitochondria by the lipophilic cationic porphyrin POR10. *J Photochem Photobiol B Biol* **34**, 191–196.
14. Batinic-Haberle I, Tovmasyan A, Spasojevic I (2015) An educational overview of the chemistry, biochemistry and therapeutic aspects of Mn porphyrins – From superoxide dismutation to H₂O₂-driven pathways. *Redox Biol* **5**, 43–65.
15. Oberley-Deegan RE, Rebets BW, Weaver MR, Tollefson AK, Bai X, McGibney M, Ovrutsky AR, Chan ED, et al (2010) An oxidative environment promotes growth of mycobacterium abscessus. *Free Radic Biol Med* **49**, 1666–1673.
16. Koyama H, Nojiri H, Kawakami S, Sunagawa T, Shirasawa T, Shimizu T (2013) Antioxidants improve the phenotypes of dilated cardiomyopathy and muscle fatigue in mitochondrial superoxide dismutase-deficient mice. *Molecules* **18**, 1383–1393.
17. Miriyala S, Spasojevic I, Tovmasyan A, Salvemini D, Vujaskovic Z, St Clair D, Batinic-Haberle I (2012) Manganese superoxide dismutase, MnSOD and its mimics. *Biochim Biophys Acta* **1822**, 794–814.
18. Kezic A, Spasojevic I, Lezaic V, Bajcetic M (2016) Mitochondria-targeted antioxidants: future perspectives in kidney ischemia reperfusion injury. *Oxid Med Cell Longev* **2016**, 2950503.
19. Antoni PM, Naik A, Albert I, Rubbiani R, Gupta S, Ruiz-Sánchez P, Munikorn P, Mateos JM, et al (2015) (Metallo)porphyrins as potent phototoxic anti-cancer agents after irradiation with red light. *Chem Eur J* **21**, 1179–1183.
20. Asayama S, Kawamura E, Nagaoka S, Kawakami H (2005) Design of manganese porphyrin modified with mitochondrial signal peptide for a new antioxidant. *Mol Pharm* **3**, 468–470.
21. Li AM, Martins J, Tovmasyan A, Valentine JS, Batinic-Haberle I, Spasojevic I, Gralla EB (2014) Differential localization and potency of manganese porphyrin superoxide dismutase-mimicking compounds in *Saccharomyces cerevisiae*. *Redox Biol* **3**, 1–6.
22. Saba H, Batinic-Haberle I, Munusamy S, Mitchell T, Lichti C, Megyesi J, MacMillan-Crow LA (2007) Manganese porphyrin reduces renal injury and mitochondrial damage during ischemia/reperfusion. *Free Radic Biol Med* **42**, 1571–1578.
23. Moini H, Packer L, Saris NEL (2002) Antioxidant and prooxidant activities of α -lipoic acid and dihydrolipoic acid. *Toxicol Appl Pharmacol* **182**, 84–90.
24. Park S, Karunakaran U, Jeoung N, Jeon JH, Lee IK (2014) Physiological effect and therapeutic application of alpha lipoic acid. *Curr Med Chem* **21**, 3636–3645.
25. Liu J (2008) The effects and mechanisms of mitochondrial nutrient α -lipoic acid on improving age-associated mitochondrial and cognitive dysfunction: an overview. *Neurochem Res* **33**, 194–203.
26. Gurkan AS, Karabay A, Buyukbingol Z, Adejare A, Buyukbingol E (2005) Syntheses of novel indole lipoic acid derivatives and their antioxidant effects on lipid peroxidation. *Arch Pharm* **338**, 67–73.
27. Tirosh O, Shilo S, Aronis A, Sen CK (2003) Redox regulation of mitochondrial permeability transition: effects of uncoupler, lipoic acid and its positively charged analog LA-plus and selenium. *Biofactors* **17**, 297–306.
28. Hiller S, DeKroon R, Xu L, Robinette J, Winnik W, Alzate O, Simington S, Maeda N, et al (2014) Alpha-lipoic acid protects mitochondrial enzymes and attenuates lipopolysaccharide-induced hypothermia in mice. *Free Radic Biol Med* **71**, 362–367.
29. Zakavi S, Mojarrad AG, Yazdely TM (2012) Facile purification of meso-tetra(pyridyl)porphyrins and detection of unreacted porphyrin upon metallation of meso-tetra(aryl)porphyrins. *Macroheterocycles* **5**, 67–71.
30. Basel Y, Hassner A (2001) Imidazole and trifluoroethanol as efficient and mild reagents for destruction of excess di-tert-butyl dicarbonate [(BOC)₂O]. *Synthesis* **4**, 550–552.
31. Liu F, Wang M, Wang Z, Zhang X (2006) Polymerized surface micelles formed under mild conditions. *Chem Commun* **2006**, 1610–1612.
32. Makpol S, Jam FA, Khor SC, Ismail Z, Yusof YAM, Ngah WZ (2013) Comparative effects of biodynes, tocotrienol-rich fraction, and tocopherol in enhancing collagen synthesis and inhibiting collagen degradation in stress-induced premature senescence model of human diploid fibroblasts. *Oxid Med Cell Longev* **2013**, 298574.
33. Boncler M, Rozalski M, Krajewska U, Podsedek A, Watala C (2014) Comparison of PrestoBlue and MTT assays of cellular viability in the assessment of anti-proliferative effects of plant extracts on human endothelial cells. *J Pharmacol Toxicol Methods* **69**, 9–16.
34. Choi IY, Lee SJ, Ju C, Nam W, Kim HC, Ko KH, Kim WK (2000) Protection by a manganese porphyrin of endogenous peroxynitrite-induced death of glial cells via inhibition of mitochondrial transmembrane potential decrease. *Glia* **31**, 155–164.
35. Chazotte B (2011) Labeling mitochondria with JC-1. *Cold Spring Harb Protoc* **2011**, 065490.
36. Institute of medicine (2001) *Dietary Reference Intakes: Vitamin A, Vitamin K, Arsenic, Boron, Chromium, Copper, Iodine, Iron, Manganese, Molybdenum, Nickel, Silicon, Vanadium, and Zinc*, National Academy Press, USA.

Appendix A. Supplementary data

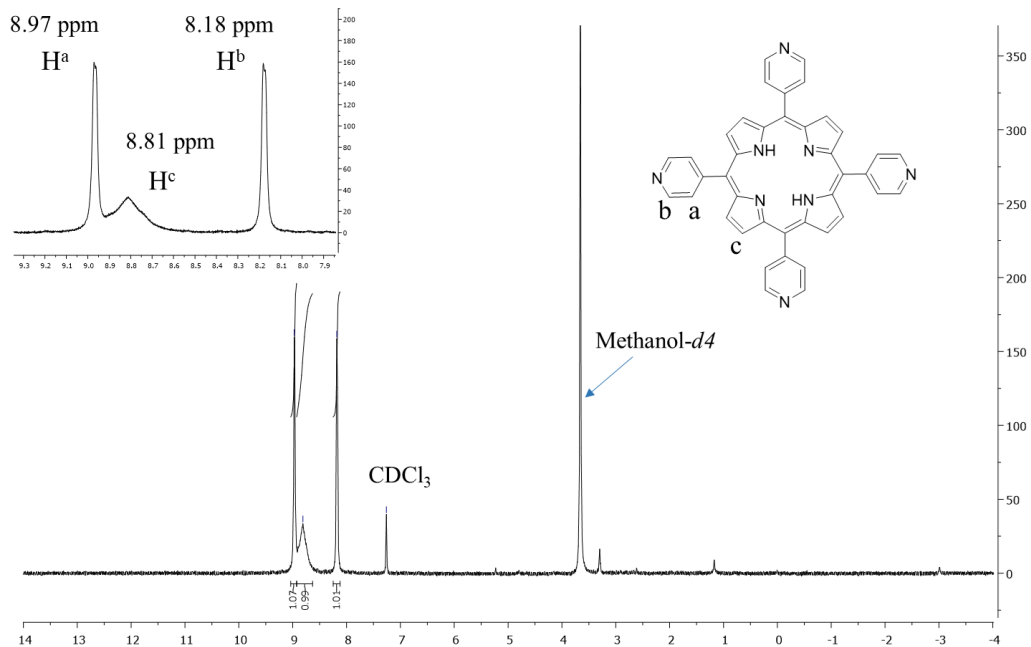


Fig. S1 ¹H-NMR spectrum of compound 1 in CDCl₃/MeOD.

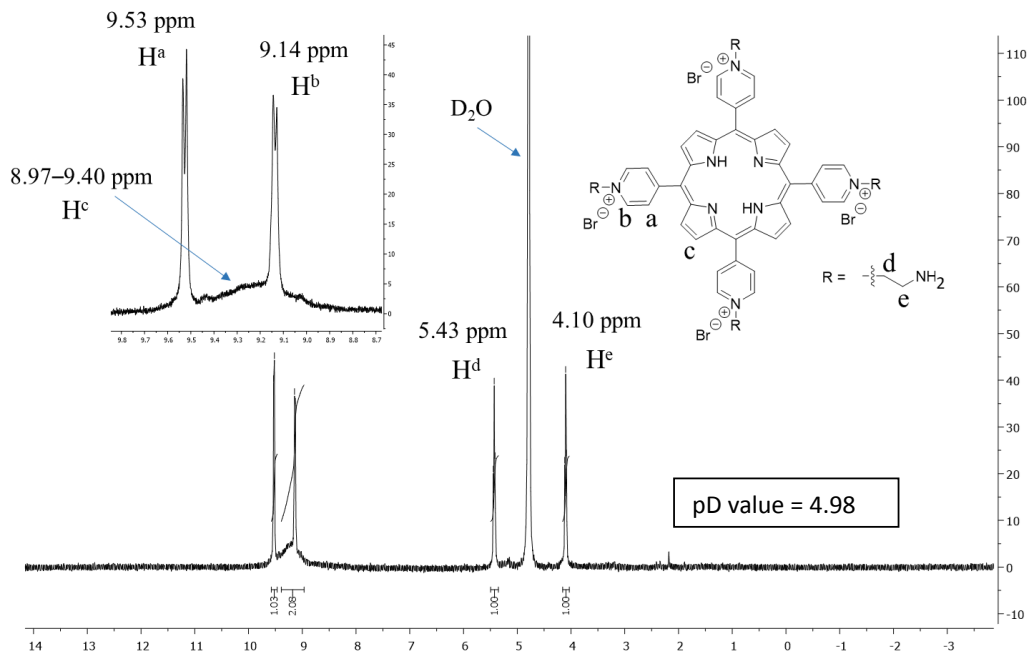


Fig. S2 ¹H-NMR spectrum of compound 2 in D₂O. The pD value is calculated from the measured pH value with the equation: pD = pH + 0.40.

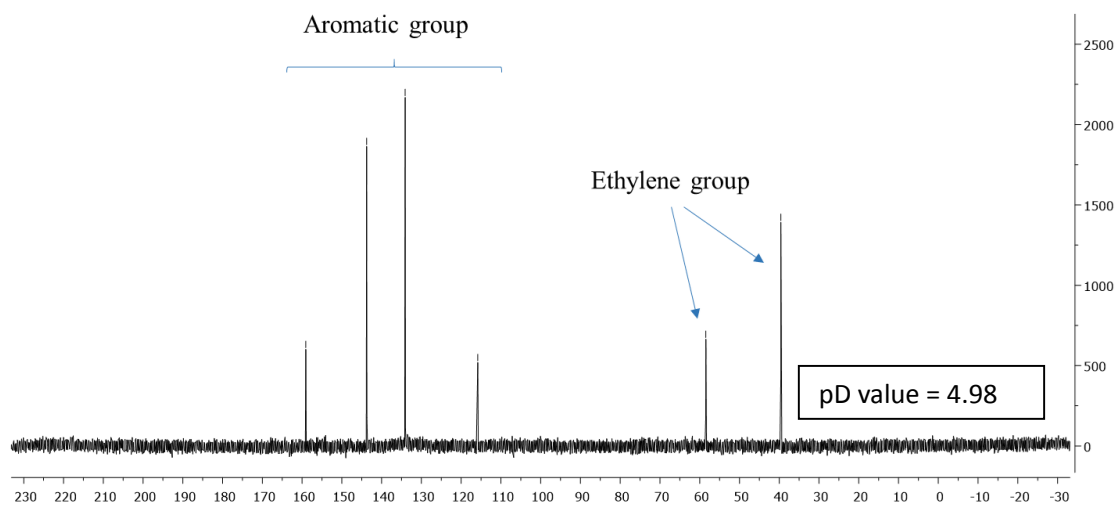


Fig. S3 ^{13}C -NMR spectrum of compound 2 in D_2O . The pD value is calculated from the measured pH value with the equation: $\text{pD} = \text{pH} + 0.40$.

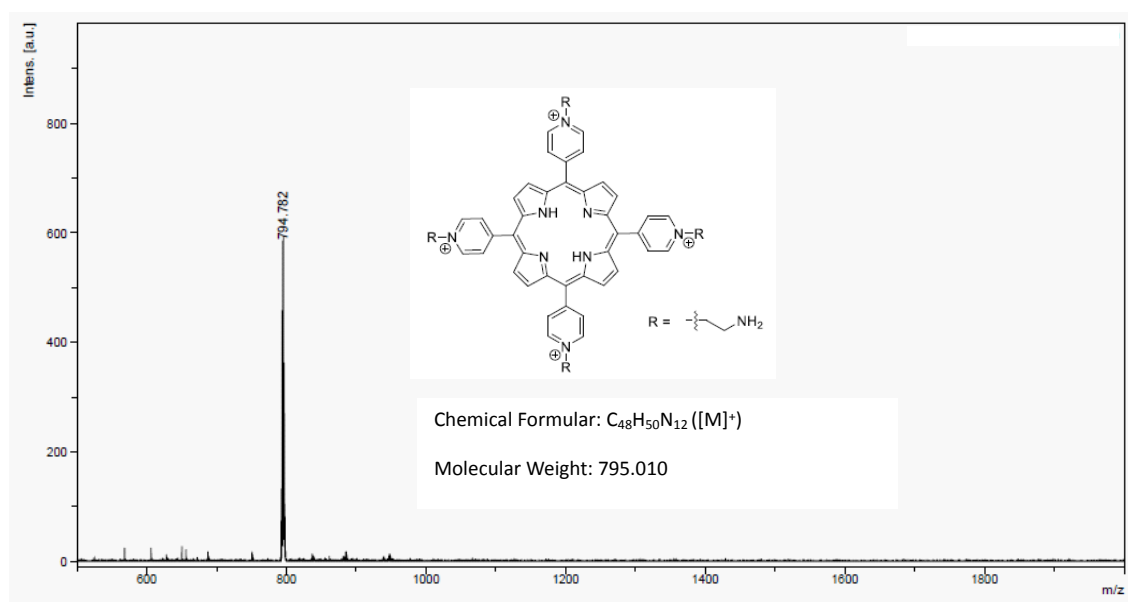


Fig. S4 MALDI-TOF-MS of compound 2.

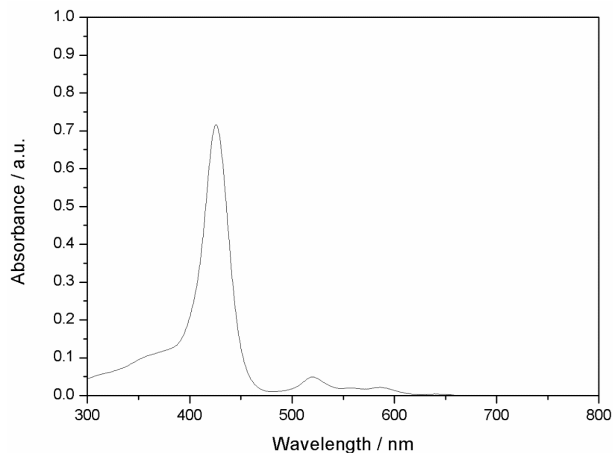


Fig. S5 Absorption spectrum of compound 2 in H₂O.

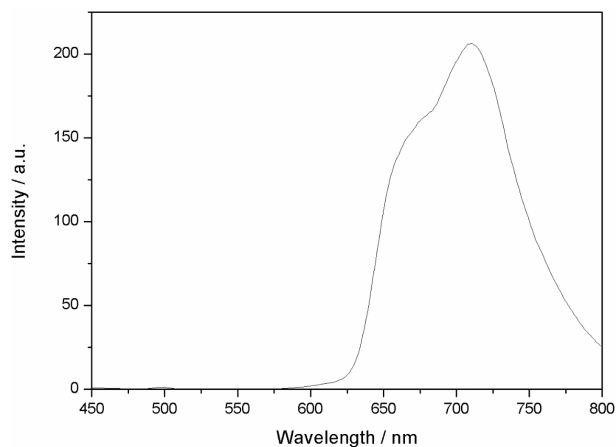


Fig. S6 Emission spectrum of compound 2 in H₂O.

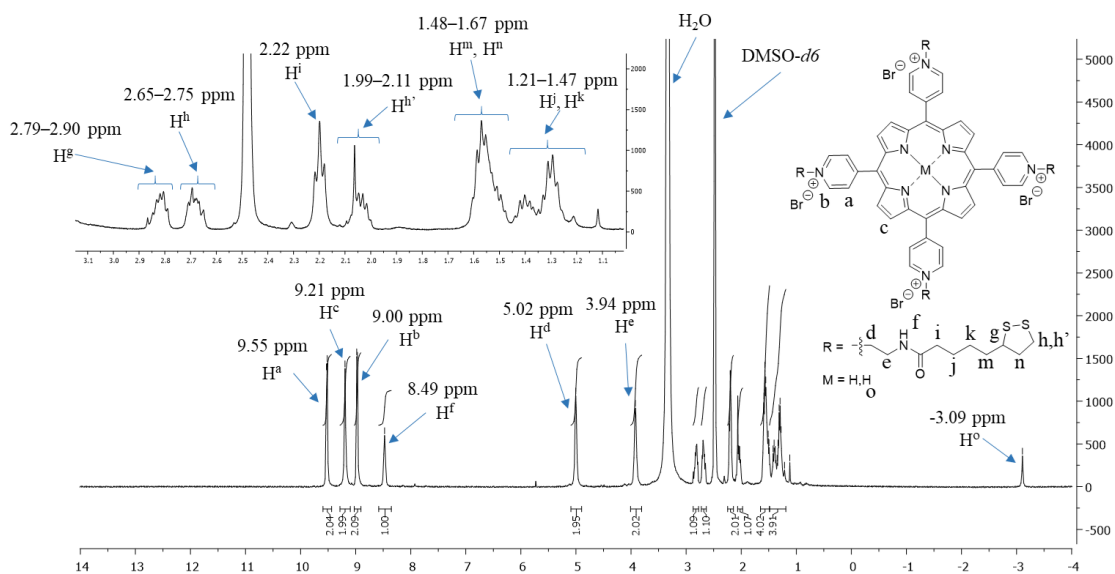


Fig. S7 ¹H-NMR spectrum of compound 3 in DMSO-*d*₆.

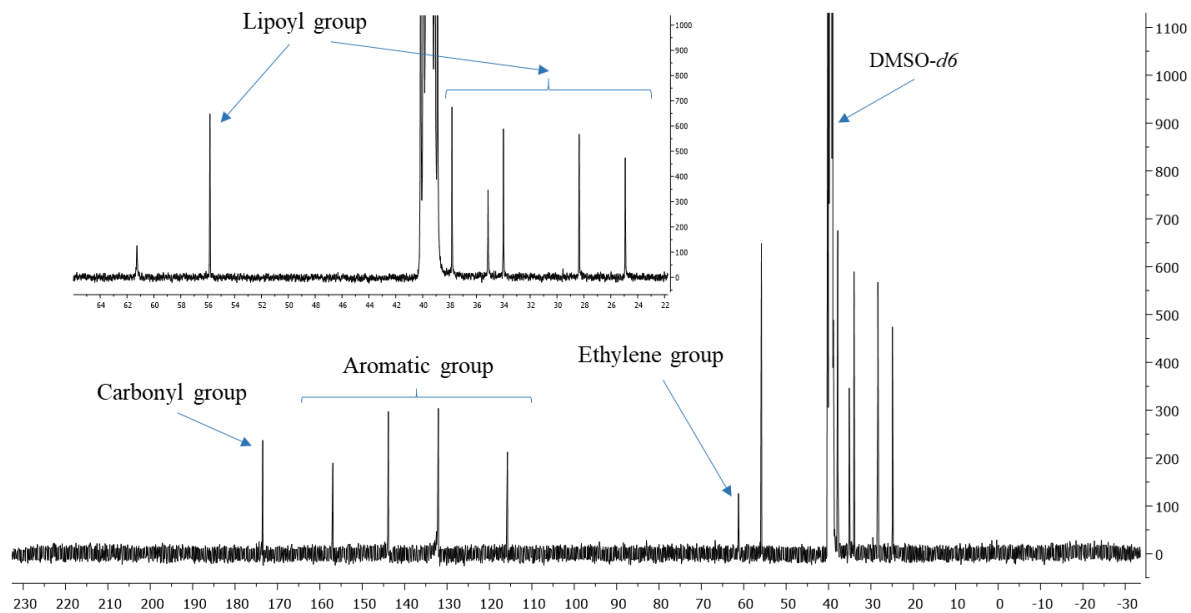


Fig. S8 $^{13}\text{C-NMR}$ spectrum of compound 3 in DMSO- d_6

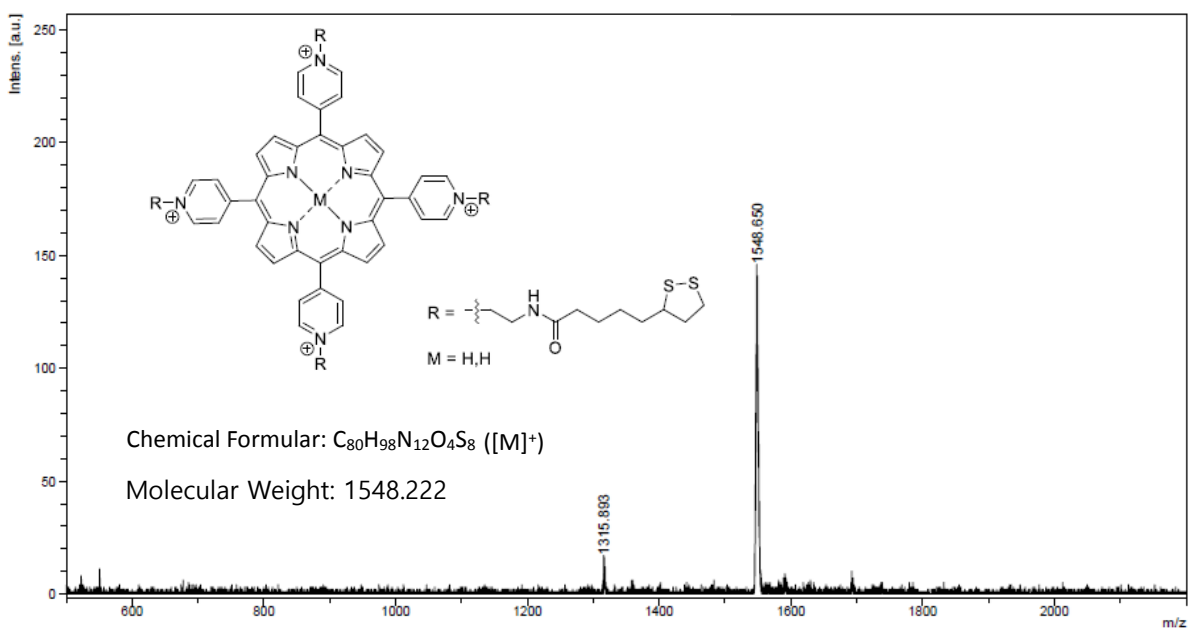


Fig. S9 MALDI-TOF-MS of compound 3.

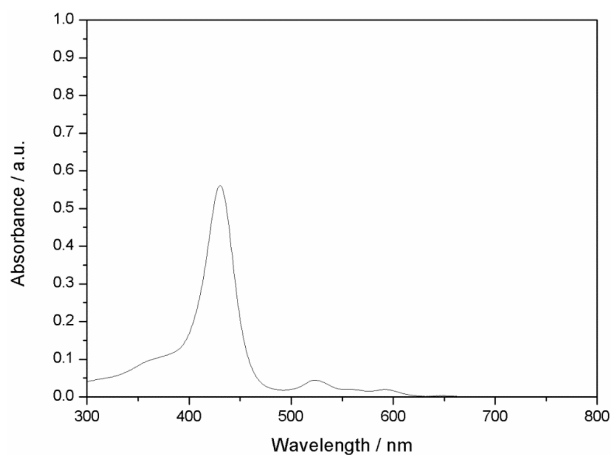


Fig. S10 Absorption spectrum of compound 3 in H₂O.

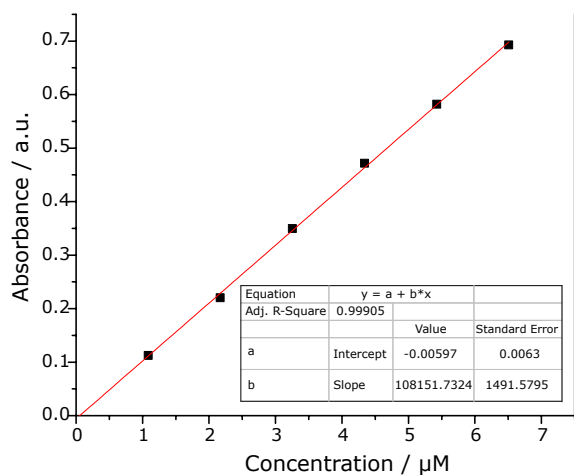


Fig. S11 Calibration curve of compound 3 in H₂O ($\lambda_{\text{abs}} = 430 \text{ nm}$).

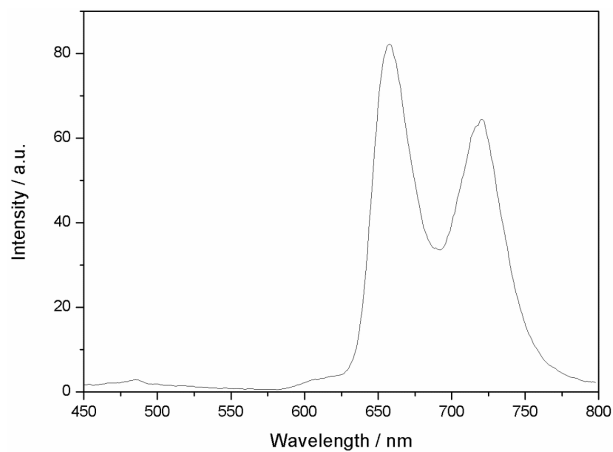


Fig. S12 Emission spectrum of compound 3 in H₂O.

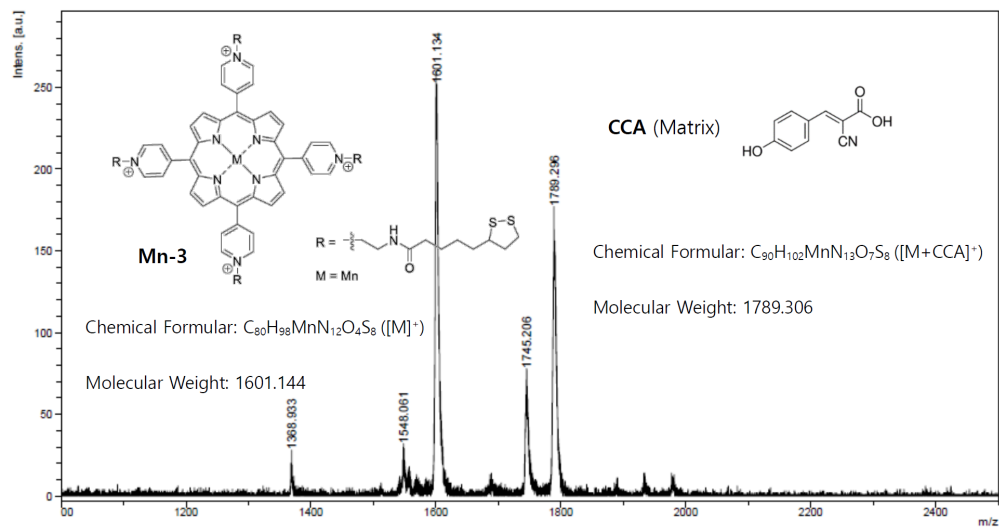
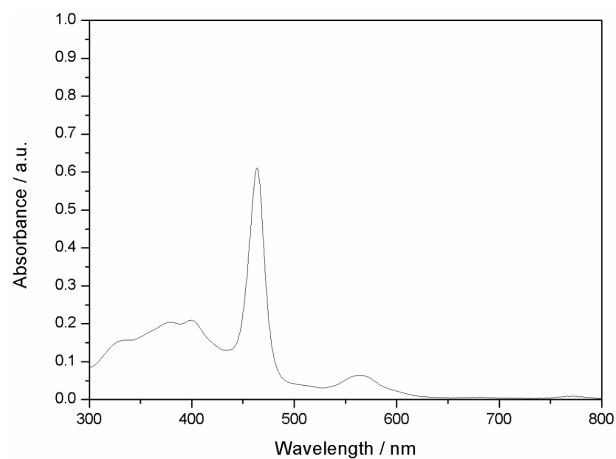
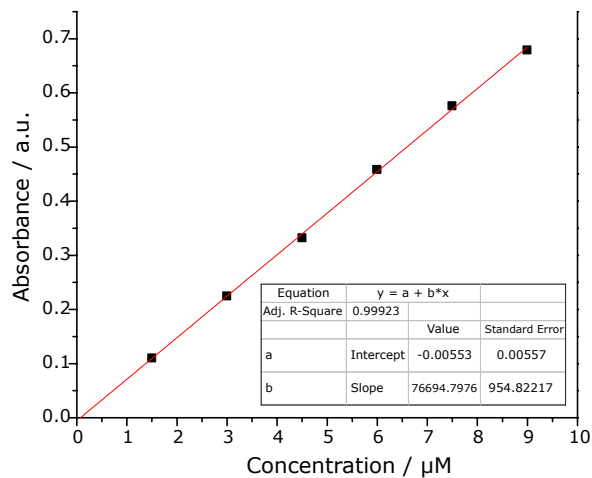


Fig. S13 MALDI-TOF-MS of compound Mn-3.

Fig. S14 Absorption spectrum of compound Mn-3 in H_2O .Fig. S15 Calibration curve of compound Mn-3 in H_2O ($\lambda_{abs} = 464$ nm).